THE JOURNAL OF PHYSICAL CHEMISTRY B LETTERS

2005, *109,* 11414−11419
Published on Web 05/21/2005

Characterization of Paramagnetic Species in N-Doped TiO_2 Powders by EPR Spectroscopy and DFT Calculations

Cristiana Di Valentin,*,†,‡ Gianfranco Pacchioni,† Annabella Selloni,‡ Stefano Livraghi,§ and Elio Giamello§

Dipartimento di Scienza dei Materiali, Università di Milano-Bicocca, Via R. Cozzi, 53, 20125 Milano, Italy, Department of Chemistry, Princeton University, Princeton, New Jersey 08540, and Dipartimento di Chimica IFM, Università di Torino and NIS, Nanostructured Interfaces and Surfaces Centre of Excellence, Via P. Giuria 7, I - 10125 Torino, Italy

Received: April 6, 2005; In Final Form: May 10, 2005

Electron paramagnetic resonance (EPR), X-ray photoelectron spectroscopy (XPS), and density functional theory (DFT) calculations are combined for the first time in an effort to characterize the paramagnetic species present in N-doped anatase TiO_2 powders obtained by sol−gel synthesis. The experimental hyperfine coupling constants are well reproduced by two structurally different nitrogen impurities: substitutional and interstitial N atoms in the TiO_2 anatase matrix. DFT calculations show that the nitrogen impurities induce the formation of localized states in the band gap. Substitutional nitrogen states lie just above the valence band, while interstitial nitrogen states lie higher in the gap. Excitations from these localized states to the conduction band may account for the absorption edge shift toward lower energies (visible region) observed in the case of N-doped TiO_2 with respect to pure TiO_2 (UV region). Calculations also show that nitrogen doping leads to a substantial reduction of the energy cost to form oxygen vacancies in bulk TiO_2. This suggests that nitrogen doping is likely to be accompanied by oxygen vacancy formation. Finally, we propose that the relative abundance of the two observed nitrogen-doping species depends on the preparation conditions, such as the oxygen concentration in the atmosphere and the annealing temperature during synthesis.

1. Introduction

A number of recent papers have reported on the photoabsorption in the visible region and the photocatalytic properties of nitrogen-doped TiO_2.[1] The reduction of the optical threshold energy of TiO_2 (pure anatase TiO_2 band gap = 3.2 eV) and the consequent possibility of using economical and ecological sunlight instead of UV irradiation in photocatalysis are expected to have tremendous implications on the technological applications of this system. Given the importance and interest of this subject, a clear rationalization of the nitrogen species present in the N-doped samples is desirable. To date, however, the mechanism of visible light response is quite confused. While some groups propose the presence of NO_x[1a,c,2−4] or NH_x[1e] species, others attribute the visible activity to substitutional nitrogen doping.

In the present work, for the first time, electron paramagnetic resonance (EPR), X-ray photoelectron spectroscopy (XPS), and density functional theory (DFT) calculations are combined in order to characterize the paramagnetic species present in N-doped anatase TiO_2 powders obtained by sol−gel synthesis. The EPR technique, at variance with other spectroscopic techniques, presents a unique sensibility which allows one to detect paramagnetic species even at very low concentration, as those typical of N-doped TiO_2 systems. These species are characterized by comparing the observed EPR hyperfine coupling constants with computed values for structural models of substitutional and interstitial nitrogen impurities. Calculated core levels and experimental XPS N (1s) features are also analyzed to corroborate the conclusions. Moreover, calculations of the N-doping-induced modifications of the TiO_2 electronic structure are found to provide support[5] to the localized nature of the N-induced electronic states.[1c,6−8] Finally, the interaction of nitrogen impurities and oxygen vacancies is briefly discussed.

2. Experimental Section

2.a. Materials and Setup. Sol−gel N-doped TiO_2 samples were prepared mixing a solution of titanium(IV) isopropoxide in isopropyl alcohol with a solution of NH_4Cl in water and keeping the mixture under constant stirring at room temperature until completed hydrolysis. The gel was left aging for 15 h at room temperature and subsequently dried at 70 °C for 2 h. The dried material was calcined in air at 770 K for 1 h. After calcination, the solid is pale yellow and exhibits the structure of the anatase polymorph.

EPR spectra were run on a Bruker EMX machine working in the X-band mode at 9.5 GHz, while the Q-band spectra at 35 GHz were run on a Bruker ESP300 machine. Computer simulations of the spectra were obtained using the SIM32 program.[9] XPS spectra were run at the Department of Chemistry (University of Cardiff) on a VG ESCALAB 220 machine.

* Corresponding author. E-mail: cristiana.divalentin@mater.unimib.it.
† Università di Milano-Bicocca.
‡ Princeton University.
§ Università di Torino and NIS.

10.1021/jp051756t CCC: $30.25 © 2005 American Chemical Society

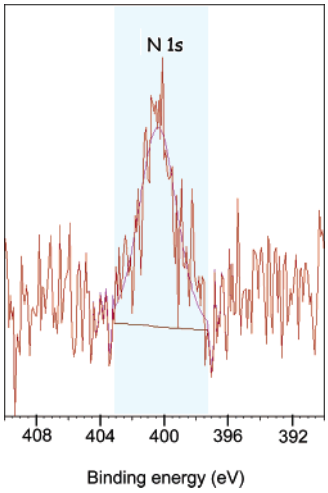

Figure 1. XPS peak centered around 400 eV recorded for N−TiO_2 (anatase phase).

2.b. XPS Results. Nitrogen-doped TiO_2 materials prepared by sol−gel reaction using ammonium chloride as a nitrogen carrier display a pale yellow color and are characterized by various spectroscopic features. In particular, an XPS peak at about 400 eV (N 1s) was observed (Figure 1). This lies in the range (396−404 eV) observed by several other authors[1b,c,e,g,2,8] and is typical of nitrogen-doped titanium dioxide. The assignment of this XPS peak is still under debate, and controversial hypotheses are found in the literature.

Various forms of N-doped TiO_2 have been investigated (powders, films, nanoparticles, and single crystals), and they were obtained following very different procedures. In most cases, a peak at 396−397 eV was detected and attributed to substitutional nitrogen doping given the proximity to the typical binding energy of 397 eV in TiN.[10] However, in a few recent papers, this feature was found to be completely absent, while peaks at higher binding energies (399−404 eV) were observed.[1c,g,2,8] In some other cases, both features have been observed.[1b,e] Since the peaks for nitrites and nitrates fall at a very high binding energy (407−408 eV), nitrogen species in doped TiO_2 are expected to be in a lower oxidation state.

We conclude this discussion with two main considerations. First, preparation methods and conditions largely affect nitrogen XPS spectral features. Second, it is highly probable that the N 1s peak observed originated from the concomitant presence of a variety of nitrogen species (also those eventually trapped in the matrix), among which the paramagnetic species are probably a minority. Indications of this come from the infrared spectrum registered for the present samples, which shows N−H bands, probably deriving from excess NH_4Cl used for the synthesis.

2.c. EPR Results. The most interesting feature of the material is that it contains N-based paramagnetic centers with a concentration of about 10^{17} spin/g. EPR spectra of paramagnetic centers in N−TiO_2 were actually reported in the past[3,11] but without a detailed discussion of their structural and spectroscopic features and a consequent convincing assignment. In a recent paper,[4] some of us reported the existence of two distinct paramagnetic species in N−TiO_2, both containing a single nitrogen atom. One of them was assigned to the nitric oxide molecular radical (NO). This molecule is encapsulated in microvoids of the solid and is observed by EPR at 77 K when it adsorbs on the walls of the cavity. Its chemical nature indicates the occurrence of a deep oxidation of the ammonium ions during the calcination of the gel.

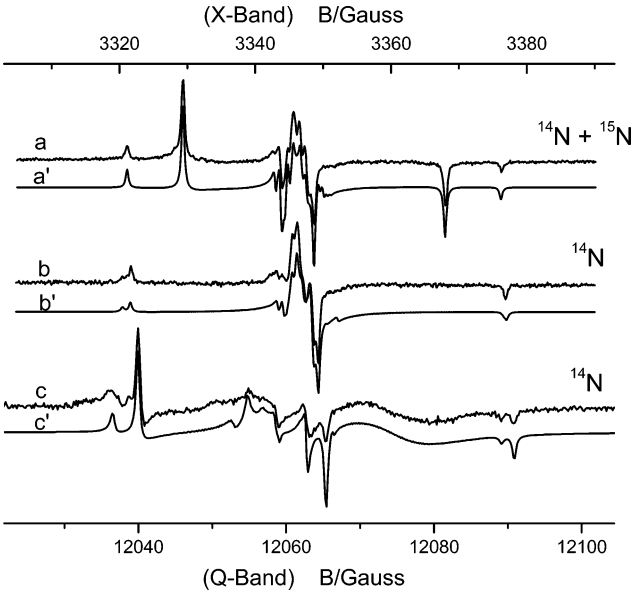

Figure 2. EPR spectra and related simulation of the N-containing paramagnetic center in N−TiO_2: (a) X-band spectrum of the species containing ^{15}N and ^{14}N (70 and 30%, respectively); (b) X-band spectrum of the species containing ^{14}N; (c) Q-band spectrum of the species containing ^{14}N.

A second N-containing species was observed by EPR at room temperature, being, at lower temperature, buried in the more intense spectrum of trapped NO. A spectrum very similar to that of this second species was observed by Che and Naccache[12] in a TiO_2 sample treated with ammonia and calcined at high temperature more than 30 years ago and prior to the discovery of N−TiO_2.[1a] The spectrum was assigned by the authors to a NO_2^{2-} species similar to that observed in irradiated nitrates.[13] Whatever its nature, this latter species is localized in the bulk of the solid and not at its surface.[4,12] Furthermore, it has a very intimate connection with the TiO_2 matrix as its spectrum disappears upon reducing the sample by annealing in vacuo at 500 K and reversibly reappears when the sample is reoxidized in oxygen.[4]

After the EPR spectra preliminarily reported in ref 4, we were able to obtain, for the species mentioned above, better resolved X-band spectra (ν = 9.5 GHz) using, in the preparation, compounds containing either ^{14}N (nuclear spin $I = 1$, multiplicity = 3) or ^{15}N ($I = {}^1/_2$, multiplicity = 2). Additionally, a Q-band spectrum (ν = 35 GHz) for the ^{14}N species was recorded. The three spectra are reported in Figure 2 with the corresponding computer simulation. The same spin-Hamiltonian parameters were used in the three simulations just scaling the coupling constants of the expected value passing from ^{14}N to ^{15}N. The satisfactory and self-consistent result of the simulation allowed us to update the set of spin-Hamiltonian parameters of the nitrogen species, not fully determined in the previous study.[4] A scrutiny of the spectra in Figure 2, however, indicates a second new fact, that is, the presence in the system of two slightly different species, one of which is 3.5−4 times more intense than the other. The case of two or more species having the same chemical nature and slightly different in the coordinative environment is rather common in solid state chemistry and leads to different spin-Hamiltonian parameters because of the high sensitivity of the latter ones to small local distortions. We will refrain therefore from speculating on this tiny difference in EPR parameters, and we will refer in the following to the more abundant of the two centers.

TABLE 1: Experimental and Computed ^{14}N Hyperfine Coupling Constants and N Atomic Spin Density

	A_1	A_2	A_3	a_{iso}	B_1	B_2	B_3	ρ_p
					$-b/-b'$	$-b/2b'$	$2b/-b'$	
exptl	2.3	4.4	32.3	13.0	−10.0/−0.7	−10.0/1.4	20.0/−0.7	54
N_{sub}	2.5	2.8	38.2	14.5	−12.0	−11.7	23.7	87
N_{int}	0.2	1.8	33.4	11.8	−11.6	−10.0	21.6	67

The species is characterized by rhombic **g** ($g_1 = 2.0054$, $g_2 = 2.0036$, and $g_3 = 2.0030$) and **A** tensors. The latter one is also reported in Table 1 and is based on a quite large coupling constant (±32.3 G) in the direction of the g_3 element and two smaller constants in the other directions ($A_1 = \pm 2.3$ G and $A_2 = \pm 4.4$ G). The same set of spin-Hamiltonian parameters was used to simulate both the X-band and Q-band spectra, obtaining a satisfactory fit between experimental and simulated traces in the two cases (Figure 2). This permits a reliable analysis of the spin density in the center based on the decomposition of the **A** matrix according to

$$\mathbf{A} = \begin{vmatrix} A_1 & & \\ & A_2 & \\ & & A_3 \end{vmatrix} = a_{iso} + \begin{vmatrix} B_1 & & \\ & B_2 & \\ & & B_3 \end{vmatrix} = a_{iso} + \begin{vmatrix} -b & & \\ & -b & \\ & & 2b \end{vmatrix} + \begin{vmatrix} -b' & & \\ & 2b' & \\ & & -b' \end{vmatrix} \quad (1)$$

where a_{iso} is the Fermi contact term. Since the experimental **B** matrix does not have the typical form of the electron−nucleus dipolar interaction for an electron in a p orbital (i.e., $-B$, $-B$, $2B$), it has been decomposed into two matrixes (based on b and b′) which have the expected structure. This indicates the existence of a contribution (b') to the dipolar interaction of a second p orbital. Both b and b' experimental values are reported in Table 1, while the calculated values of the dipolar hyperfine interaction are reported in the aggregated form (B). The spin density in the p orbitals, calculated by comparison of the experimental values with the corresponding atomic value ($\rho_{2p} = 2b/B°$), is thus mainly localized (0.505) on one N 2p orbital with a minor contribution (0.035) of a second one (b'). The isotropic Fermi contact term is expected to be positive in N-centered radical species and indicates a further amount of electron spin density (0.02) in the 2s nitrogen orbital. The total spin density on the N atom of the observed species amounts therefore to 0.56, with the larger contribution being due to a single p orbital of the nitrogen atom in the center.

The previous analysis indicates that the hyperfine tensor does not account for the whole unpaired electron spin density. In most cases of molecular radical centers, the unaccounted spin density is usually localized on other atoms of the species having zero nuclear spin. In particular circumstances, however, the presence of diffuse electronic states with excited state character can produce a reduction of the hyperfine constants not due to an effective spin delocalization on other atoms. In this latter case, the comparison of the experimental hyperfine constants with the tabulated atomic value is, of course, meaningless.

3. Theoretical Section

3.a. Computational Details. The calculations have been performed using the plane-wave-pseudopotential approach together with the Perdew−Burke−Ernzerhof (PBE)[14] exchange-correlation functional and ultrasoft pseudopotentials[15] (with kinetic energy cutoffs of 25 and 200 Ry for the smooth part of the electronic wave functions and augmented electron density, respectively). The ν-ESPRESSO package[16] was employed: the Car−Parrinello (CP) approach[17,18] was used for geometry optimizations, with the Brillouin zone sampling limited to the Γ point, while the PWSCF code was used to perform calculations at a low-symmetry k-point and obtain electronic band structures, spin density maps, and the energetics of processes. The supercell used is a 96-atom almost cubic anatase $2\sqrt{2} \times 2\sqrt{2} \times 1$ supercell. Substitutional N-doping was modeled by replacing one oxygen atom in the supercell, while interstitial N-doping was modeled by adding one N atom in the supercell. When studying oxygen vacancy formation, one oxygen atom was removed while two other oxygen atoms were replaced with nitrogen atoms. Atomic relaxations were carried out using a second-order damped dynamics until all components of the residual forces were less than 0.025 eV/Å. When examining the relative positions of the valence and conduction band edges and impurity states, the Ti 3s levels have been aligned to each other, since they are at the same energy in pure and N-doped anatase TiO_2. Further details on the computational setup were reported in a previous work.[5]

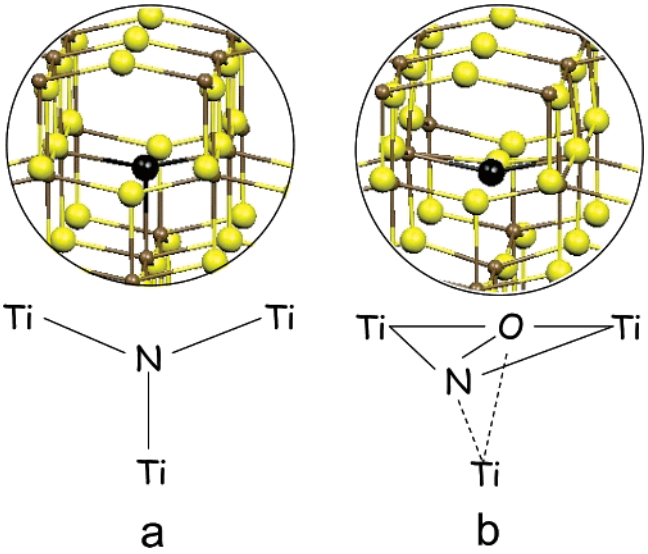

Figure 3. Partial geometry and schematic sketch of the model for (a) substitutional and (b) interstitial N-doping in an anatase matrix. The N atom is represented by a black sphere, O atoms are represented by yellow spheres, and Ti atoms are represented by small brown spheres.

To compute atomic spin properties, such as the hyperfine coupling constants of the electron spin with the nuclear spin of ^{14}N and atomic spin densities, we used the CRYSTAL03 program package,[19] based on an atomic orbital basis set together with the Becke-3[20] and Lee−Yang−Parr[21] (B3LYP) exchange and correlation functional. Hybrid functionals are indeed known to give more accurate descriptions of spin-polarized systems.[22] We performed single point B3LYP calculations using the Γ point and the geometries given by the PBE calculations, with TOLINTEG (truncation criteria for bielectronic integrals) criteria: 10^{-6}, 10^{-6}, 10^{-6}, 10^{-6}, and 10^{-12}. The atoms were described with the following basis sets: Ti 86411(d41),[23] O 8411(d1),[24] N 7311(d1),[25] respectively. The hyperfine spin-Hamiltonian, $H_{hfc} = S\cdot\mathbf{A}\cdot I$, is given in terms of the hyperfine matrix **A** which describes the coupling of the electron with the nuclear spin; see eq 1.[26]

3.b. Model Structures. In this section, we focus our attention on possible models capable of explaining the observed properties of the nitrogen species. We have considered two models in our DFT calculations, namely, substitutional (Figure 3a) and interstitial (Figure 3b) nitrogen impurities in the anatase bulk

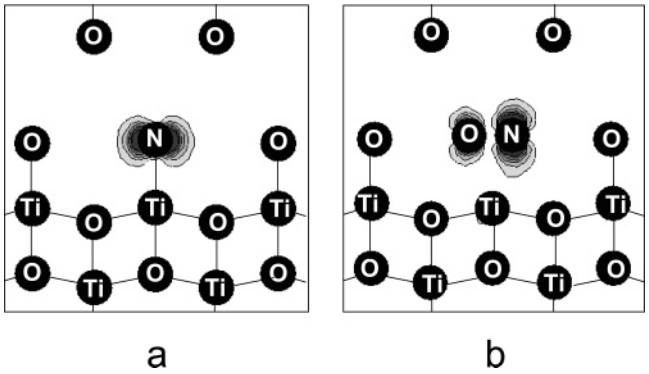

Figure 4. Spin density maps of the unpaired electron for (a) substitutional and (b) interstitial N-doped anatase TiO_2. The plot is in the plane perpendicular to that containing the three Ti atoms bound to the N species, shown in Figure 3.

structure. In the substitutional model, the nitrogen atom is bound to three Ti atoms and replaces a lattice oxygen in TiO_2. This nitrogen atom is in a negative oxidation state, and given the covalent character of the bond, its charge, which should formally be −2, is actually reduced to about −1, which is the accepted value of the charge of oxygen atoms in TiO_2.[27,28] This result is nicely confirmed by present CRYSTAL03 calculations on the basis of Mulliken population analysis. In the interstitial model, the nitrogen atoms are bound to one or more oxygen atoms and therefore are in a positive oxidation state which could range from that typical of a hyponitrite species (NO^-) to that of nitrite (NO_2^-) and nitrate species (NO_3^-). Various starting configurations for an interstitial nitrogen have been considered, with the N atom coordinated to one or up to three lattice oxygens. The lowest energy minimum is represented by the N atom bound to one lattice oxygen, forming a NO species (d(N−O) = 1.36 Å), which interacts with the lattice Ti atoms through its π bonding states (Figure 3b). We also considered the possibility of an interstitial NO species trapped in the lattice and bound to a lattice oxygen atom (NO_2^{2-}), as recently proposed on the basis of EPR measurements by Livraghi et al.[4] However, this turned out to be unstable because of the repulsive interactions of the trapped NO with the surrounding cavity. These results are consistent with the very small binding energies which have been obtained in previous calculations for NO species adsorbed on low-coordinated oxygen atoms on the surface of TiO_2.[29]

3.c. Core Level Shifts and Hyperfine Coupling Constants. Even though core level binding energy values for the N 1s state, computed within the initial state approximation, cannot be directly compared to experimental XPS data because of the absence of final state relaxation effects, the relative values of substitutional versus interstitial configurations are qualitatively relevant. The calculated values for these two species differ by 1.6 eV, with a higher core level binding energy for the interstitial configuration. This result nicely correlates with the two experimentally observed peaks for N-doped TiO_2, one at 397 eV (attributed to substitutional N) and the other at >399 eV (interstitial N).

A more accurate analysis can be performed for the spin properties, by comparing the computed and measured hyperfine coupling constants (**A** matrix in Table 1). The agreement is quite satisfactory for both the N substitutional and N interstitial configurations. In the former case, the unpaired electron is almost entirely (0.87) localized on the substitutional N atom, more precisely on the p state perpendicular to the plane defined by the three Ti atoms to which nitrogen is bound (Figure 4a). In the case of interstitial nitrogen, the unpaired electron is shared between the N and O atoms of the NO species and the

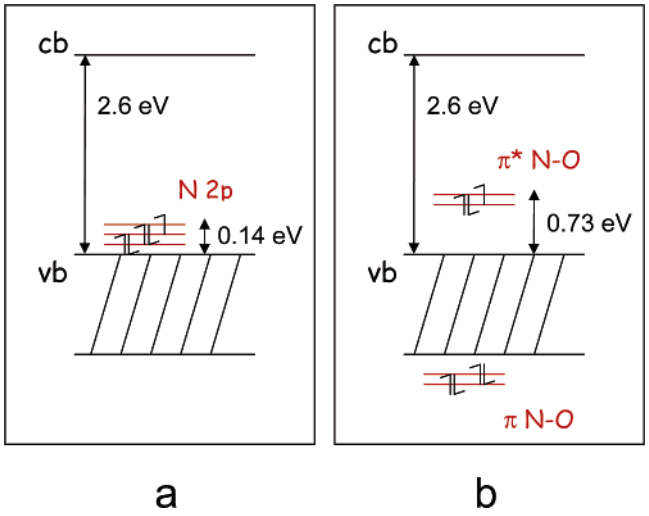

Figure 5. Electronic band structure for (a) substitutional and (b) interstitial N-doped anatase TiO_2, as given by PBE calculations at a low-symmetry k-point. The calculated value of the band gap is also reported.

localization on N is reduced to 0.67. Here, the spin density is localized on the π system of the NO species (Figure 4b) involving only p-type N atomic states. Despite the different calculated spin densities on the N atom of the two model species (0.87 and 0.67), the corresponding hyperfine coupling constants are quite similar in the two cases and rather close to the experimental values as well (see Table 1). However, as mentioned above, the spin density on N, obtained as the ratio of the experimentally measured b values with tabulated atomic $B°$ (0.54), might not be strictly correct, so that it cannot be used to discriminate between the two model species under investigation. Therefore, the above comparative experimental−computational EPR analysis indicates that both proposed models, substitutional and interstitial doping nitrogen atoms, may account for the paramagnetic species observed in the TiO_2 powders.

3.d. Electronic Structure. Recently, a lively discussion on the nature of the nitrogen-induced states has appeared in the literature.[1c,5−8] In particular, a number of experimental papers have questioned the original explanation of N-doped TiO_2 visible light photoactivity as being due to a rigid valence band shift.[1b] In these experimental studies, several indications have been presented that the electronic transition following visible light irradiation cannot be a band-to-band transition but must involve a transition from localized states to the conduction band. In a previous paper,[5] we provided theoretical evidence that indeed, in the case of substitutional N-doped anatase TiO_2, the visible light responses arise from occupied N 2p localized states slightly above the valence band edge (Figure 5a). Here, we want to compare the computed electronic band structure (at a low-symmetry k-point) of the newly optimized interstitial N species with that of substitutional nitrogen.

The NO bond generates localized states with π character (Figure 5b). The two bonding states are deep in energy and lie below the top of the O 2p band. The two antibonding (but still occupied) states lie above the O 2p band and are higher in the gap than the N 2p states generated by substitutional nitrogen: the highest localized state for the interstitial species is 0.73 eV above the top of the valence band, while for the substitutional species, it is 0.14 eV above it.[5] The computed band gap for these systems is 2.6 eV, obtained as the difference between conduction and valence band energy eigenvalues (the underestimation of band gaps is a well-known limitation of DFT).[30] Thus, the conclusion is that both N-doping configurations induce

the formation of localized occupied states in the gap, accounting for the visible light activity of N-doped samples. The localized nature of the N-induced states has the consequence that the hole generated by visible irradiation is less mobile than that generated by UV irradiation. In particular, the interstitial N impurities, which give rise to high states in the gap, might behave as stronger hole trapping sites, reducing the direct oxidation power of the sample in the photocatalytic process.[8,31]

3.e. N-Doping and Oxygen Vacancies. It is interesting to investigate whether the concomitant presence of N impurities and O vacancies may lead to some special effects. To this end, we have analyzed the effect of removing one oxygen atom in the presence of two nearby substitutional nitrogen atoms in bulk anatase. We found that the two excess electrons deriving from the oxygen vacancy (which would form Ti^{3+} states below the conduction band in undoped TiO_2) become trapped at the two N impurities, thus completely filling their 2p states. This electron transfer also causes spin quenching of the sample, since the unpaired electrons on the substitutional N atoms are paired with the excess electrons from the oxygen vacancy.

Another important consequence of the nitrogen doping is the large reduction in the cost of formation of an oxygen vacancy. While for bulk anatase the oxygen vacancy formation energy is 4.2 eV,

$$TiO_2 \rightarrow TiO_{2-x} + xV_0 + {}^1/_2 xO_2 \qquad \Delta E = 4.2 \text{ eV} \quad (2)$$

we find a vacancy formation energy as low as 0.6 eV when all excess electrons associated to O vacancies are trapped at N-impurity sites, that is,

$$TiO_{2-2x}N_{2x} \rightarrow TiO_{2-3x}N_{2x} + xV_0 + {}^1/_2 xO_2 \qquad \Delta E = 0.6 \text{ eV} \quad (3)$$

As the oxygen vacancy formation cost is reduced in the presence of nitrogen doping, also the cost of substitution of oxygen atoms with nitrogen atoms is reduced in the presence of oxygen vacancies:

$$TiO_2 + xN_2 \rightarrow TiO_{2-2x}N_{2x} + xO_2 \qquad \Delta E = 10.0 \text{ eV} \quad (4)$$

$$TiO_{2-x} + xN_2 \rightarrow TiO_{2-3x}N_{2x} + xO_2 \qquad \Delta E = 6.4 \text{ eV} \quad (5)$$

We calculated a similar effect also for the rutile polymorph: the oxygen vacancy formation energy drops from 4.3 to 1.0 eV upon nitrogen doping, while the cost for oxygen substitution with nitrogen drops from 9.7 to 6.4 eV.[32] Thus, these computational results suggest that most likely nitrogen doping is accompanied by oxygen vacancy formation, with a consequent reduction of the number of paramagnetic nitrogen species. This hypothesis may account for the above-mentioned observation that the EPR spectrum disappears upon reducing the sample by annealing in vacuo at 500 K and reversibly reappears when the sample is reoxidized in oxygen.

4. Concluding Remarks

In nitrogen-doped titanium dioxide, a paramagnetic N-based defect is observed, which is intimately bound to the bulk of the oxide and whose EPR spectral features are fully described by means of X-band and Q-band spectra and by the isotopic substitution of ^{14}N with ^{15}N. The high resolution of these spectra allowed the complete determination of the set of spin-Hamiltonian parameters of the nitrogen defect species. The experimental results have been next compared to first-principles theoretical calculations for both substitutional and interstitial nitrogen impurities. These two species, even though structurally different, were found to present similar hyperfine coupling parameters, in good agreement with the experimental data. Moreover, the possible assignment of the N defect to a NO_2^{2-} radical ion (a NO molecule bound to a lattice oxygen) was discarded, since this species was computed to be unstable in bulk TiO_2.

The characterization of substitutional or interstitial N atoms in TiO_2 by comparison of EPR spectroscopy with DFT calculations represents a new and original approach to unraveling the complex problem of the interaction of nitrogen with a titanium dioxide matrix. Despite its rather low concentration, the identified species cannot be considered (in qualitative terms) a minor byproduct of the synthesis, since it is very stable, up to very high temperatures.

The computed electronic band structures for both of the N-doped model systems indicate the formation of localized states in the band gap. Substitutional nitrogen states lie just above the valence band, while interstitial nitrogen states lie higher in the gap. Excitation from these occupied high-energy states to the conduction band can account for the optical absorption edge shift toward the lower energies (in the visible region) with respect to pure TiO_2 (UV region). However, the effective involvement of the nitrogen impurities in the photocatalytic activity in the visible region by nitrogen-doped TiO_2 should be further investigated.

An important and unexpected effect of N-doping in a TiO_2 matrix is the large decrease in the formation energy of an oxygen vacancy (from 4.2 to 0.6 eV). The consequence of this is that oxygen vacancies are probably induced by nitrogen doping of TiO_2. Also, coupling of unpaired electrons from the nitrogen impurities and from the oxygen vacancies causes spin quenching of the sample in agreement with what was experimentally observed upon annealing of the solid under vacuum (see section 2.c).

A last comment should be made on the relative stability of the two nitrogen-doping species proposed in the present work. Going from the substitutional to the interstitial nitrogen species corresponds to an oxidative process. This process is exothermic by about 0.8 eV, according to our calculations. Also, from the reverse point of view, it means that there is a cost to induce substitutional nitrogen formation starting from the interstitial one. One discriminating factor may be the reaction conditions. In excess of oxygen and nitrogen, interstitial nitrogen doping is definitely preferred. However, under highly reducing conditions, as it is after annealing at high temperature, substitutional nitrogen species in parallel with oxygen vacancies could be favored.

Acknowledgment. The authors wish to thank Dr. A. F. Carley, Dr. D. M. Murphy, and Ms. Emma Richards of the Department of Chemistry (Cardiff University, U.K.) for kindly recording the XPS spectra reported in the present paper and Dr. Lucia Bonoldi (Polimeri Europa, Novara) for recording the Q-band spectra.

References and Notes

(1) (a) Sato, S. *Chem. Phys. Lett.* **1986**, *123*, 126. (b) Asahi, R.; Morikawa, T.; Ohwaki, T.; Aoki, K.; Taga, Y. *Science* **2001**, *293*, 269. (c) Sakthivel, S.; Janczarek, M.; Kisch, H. *J. Phys. Chem. B* **2004**, *108*, 19384. (d) Irie, H.; Watanabe, Y.; Hashimoto K. *J. Phys. Chem. B* **2003**, *107*, 5483. (e) Diwald, O.; Thompshon, T. L.; Zubkov, T.; Goralski, E. G.; Walck, S. D.; Yates, J. T., Jr. *J. Phys. Chem. B* **2004**, *108*, 6004. (f) Miyauchi, M.; Ikezawa, A.; Tobimatsu, H.; Irie, H.; Hashimoto, K. *Phys. Chem. Chem. Phys.* **2004**, *6*, 865. (g) Gole, J. L.; Stout, J. D.; Burda, C.; Lou, Y.; Chen, X. *J. Phys. Chem. B* **2004**, *108*, 1230.

(2) Chen, X.; Burda, C. *J. Phys. Chem. B* **2004**, *108*, 15446.
(3) Sakatani, Y.; Nunoshige, J.; Ando, H.; Okusako, K.; Koike, H.; Takata, T.; Kondo, J. N.; Hara, M.; Domen, K. *Chem. Lett.* **2003**, *32*, 1156.
(4) Livraghi, S.; Votta, A.; Paganini, M. C.; Giamello, E. *Chem. Commun.* **2005**, *498*.
(5) Di Valentin, C.; Pacchioni, G.; Selloni, A. *Phys. Rev. B* **2004**, *70*, 085116.
(6) Lindgren, T.; Mwabora, J. M.; Avendaño, E.; Jonsson, J.; Hoel, A.; Granqvist, C.-G.; Lindquist, S.-E. *J. Phys. Chem. B* **2003**, *107*, 5709.
(7) Irie, H.; Watanabe, Y.; Hashimoto, K. *J. Phys. Chem. B* **2003**, *107*, 5483.
(8) Nakamura, R.; Tanaka, T.; Nakato, Y. *J. Phys. Chem. B* **2004**, *108*, 10617.
(9) Adamski, A.; Spalek, T.; Sojka, Z. *Res. Chem. Indermed*. **2003**, *29*, 793.
(10) Saha, N. C.; Tompkins, H. G. *J. Appl. Phys.* **1992**, *72*, 3072.
(11) Teramura, K.; Tanaka, T.; Funabiki, T. *Chem. Lett.* **2003**, *32*, 1184.
(12) Che, M.; Naccache, C. *Chem. Phys. Lett.* **1971**, *8*, 45.
(13) Atkins, P. W.; Symons, M. C. R. *The Structure of Inorganic Radicals*; Elsevier: Amsterdam, The Netherlands, 1967.
(14) Perdew, J. P.; Burke, K.; Ernzerhof, M. *Phys. Rev. Lett.* **1996**, *77*, 3865.
(15) Vanderbilt, D. *Phys. Rev. B* **1990**, *41*, 7892.
(16) Baroni, S.; dal Corso, A.; de Gironcoli, S.; Giannozzi, P.; Cavazzoni, C.; Ballabio, G.; Scandolo, S.; Chiaretti, G.; Focher, P.; Pasquarello, A.; Laasonen, K.; Trave, A.; Car, R.; Marzari, N.; Kokalj, A. http://www.pwscf.org.
(17) Car, R.; Parrinello, M. *Phys. Rev. Lett.* **1985**, *55*, 2471.
(18) Laasonen, K.; Pasquarello, A.; Car, R.; Lee, C.; Vanderbilt, D. *Phys. Rev. B* **1993**, *47*, 10142.
(19) Saunders: V. R.; Dovesi, R.; Roetti, C.; Orlando, R.; Zicovich-Wison, C. M.; Harrison, N. M.; Doll, K.; Civalleri, B.; Bush, I. J.; D'Arco, Ph.; Llunell, M. *CRYSTAL03*.
(20) Becke, A. D. *J. Chem. Phys.* **1993**, *98*, 5648.
(21) Lee, C.; Yang, W.; Parr, R. G. *Phys. Rev. B* **1988**, *37*, 785.
(22) Pacchioni, G.; Frigoli, F.; Ricci, D.; Weil, J. A. *Phys. Rev. B* **2001**, *63*, 054102.
(23) Zicovich-Wilson, C. M.; Dovesi, R. *J. Phys. Chem. B* **1998**, *102*, 1411.
(24) Ruiz, E.; Llunlell, M.; Alemany, P. *J. Solid State Chem.* **2003**, *176*, 400.
(25) Padey, R.; Jaffe, J. E.; Harrison, N. M. *J. Phys. Chem. Solids* **1994**, *55*, 1357.
(26) Weil, J. A.; Bolton, J. R.; Wertz, J. E. *Electron Paramagnetic Resonance*; Wiley: New York, 1994.
(27) Bredow, T.; Aprà, E.; Catti, M.; Pacchioni, G. *Surf. Sci.* **1998**, *418*, 150.
(28) Heise, R.; Courths, R. *Solid State Commun.* **1992**, *84*, 599.
(29) (a) Sorescu, D. C.; Rusu, C. N.; Yates, J. T., Jr. *J. Phys. Chem. B* **2000**, *104*, 4408. (b) Mguig, B.; Calatayud, M.; Minot, C. *Surf. Rev. Lett.* **2003**, *10*, 175.
(30) The band gap is not underestimated when hybrid functionals are used; for example, the computed gap is 3.9 eV with the B3LYP functional. However, the energies of the N 2p states are not significantly different when using B3LYP: 0.10 eV (vs 0.14 eV with PBE) and 0.64 eV (vs 0.73 eV with PBE) for substitutional and interstitial nitrogen, respectively.
(31) Mrowetz, M.; Balcerski, W.; Colussi, A. J.; Hoffmann, M. R. *J. Phys. Chem. B* **2004**, *108*, 17269.
(32) For the rutile polymorph, geometry optimizations have been obtained at a low-symmetry *k*-point.